

# Electroweak $W^+W^-jj$ production at NLO in QCD matched with parton shower in the POWHEG-BOX

---

**Barbara Jäger**

*PRISMA Cluster of Excellence & Institute of Physics, Johannes Gutenberg University,  
55099 Mainz, Germany*

*E-mail: jaegerba@uni-mainz.de*

**Giulia Zanderighi**

*Rudolf Peierls Centre for Theoretical Physics, 1 Keble Road, University of Oxford, UK*

*E-mail: g.zanderighi@physics.ox.ac.uk*

**ABSTRACT:** We present an implementation of electroweak  $W^+W^-jj$  production at hadron colliders in the POWHEG framework, a method that allows the interfacing of a next-to-leading order QCD calculation with parton shower Monte Carlo programs. We provide results for both, fully and semi-leptonic decay modes of the weak bosons, taking resonant and non-resonant contributions and spin correlations of the final-state particles into account. To illustrate the versatility of our implementation, we provide phenomenological results for two representative scenarios with a light and with a heavy Higgs boson, respectively, and in a kinematic regime of highly boosted gauge bosons. The impact of the parton shower is found to depend on the setup and the observable under investigation. In particular, distributions related to a central-jet veto are more sensitive to these effects. Therefore the impact of radiation by the parton shower on next-to-leading order predictions should be assessed carefully on a case-by-case basis.

**KEYWORDS:** POWHEG, NLO, QCD, SMC.

---

## Contents

<b>1. Introduction</b>	<b>1</b>
<b>2. Technical details</b>	<b>2</b>
2.1 Next-to-leading order QCD corrections to VBF $W^+W^-jj$ production	2
2.2 The POWHEG BOX implementation	4
<b>3. Phenomenological results</b>	<b>6</b>
3.1 Results at 8 TeV	7
3.1.1 Fully leptonic decay mode	7
3.1.2 Semi-leptonic decay mode	11
3.2 Semi-leptonic decay mode with boosted kinematics	13
<b>4. Conclusions</b>	<b>14</b>

---

## 1. Introduction

With the discovery of a new particle that is compatible with the postulated Higgs boson at the CERN Large Hadron Collider (LHC) [1,2] and evidence for its existence at the Fermilab Tevatron [3], high-energy physics has entered a new era. To clarify whether this particle with a mass of about 125 GeV indeed is the CP-even, spin-zero Higgs boson predicted by the Standard Model (SM), a determination of its properties, such as its couplings to gauge bosons and fermions, spin and CP properties, and decay width, is indispensable [4–6].

In this context, electroweak vector boson fusion (VBF) processes play a crucial role [7–10]. Higgs production via VBF mainly proceeds via the scattering of quarks by the exchange of weak gauge bosons in the  $t$ -channel that subsequently radiate a Higgs boson. Because of the color singlet nature of the weak gauge boson exchange, gluon radiation in the central-rapidity region is strongly suppressed. The scattered quarks typically give rise to two well-separated jets in the forward regions of the detector, while the decay products of the Higgs boson tend to be located at central rapidities, in between the two tagging jets. These characteristic features of VBF reactions help to distinguish them from a priori overwhelming QCD backgrounds. Higgs production via VBF has been considered in the  $H \rightarrow \gamma\gamma$ ,  $H \rightarrow \tau^+\tau^-$ , and the fully leptonic  $H \rightarrow WW^{(*)}$  decay modes in the most recent analyses of the ATLAS [1] and CMS collaborations [2]. Clearly, a precise knowledge of each signal and background process is essential for quantitative results, in particular if one aims at performing coupling measurements.

In this article, we focus on electroweak  $W^+W^-$  production in association with two tagging jets,  $pp \rightarrow W^+W^-jj$ . This process contains both, the signal-type contributions

from the VBF-induced production of a Higgs boson that subsequently decays into a pair of weak bosons, and the irreducible background from the continuum  $W^+W^-$  production via VBF. To maintain unitarity, both contributions to the full  $W^+W^-jj$  final state at order  $\mathcal{O}(\alpha^4)$  have to be taken into account, even though in experimental analyses selection cuts may be imposed to diminish the impact of the unwanted background coming from the  $W^+W^-$  continuum. In order to best tune the selection cuts, it is then clearly desirable to be able to simulate the VBF-induced  $W^+W^-jj$  production at the Higgs resonance as well as in the  $W^+W^-$  continuum in a common setup, taking both types of contributions consistently into account at the highest level of precision that is currently attainable for this class of reactions [11–16]. Accomplishing this goal is the major purpose of this work. Building on existing next-to-leading order (NLO) QCD calculations for weak boson pair production via VBF [11], we aim at providing an interface between the NLO-QCD calculation and parton shower programs such as HERWIG [17, 18] or PYTHIA [19] to allow for precise, yet realistic and flexible simulations of  $W^+W^-jj$  production processes at hadron colliders. To this end we develop an implementation of electroweak  $W^+W^-jj$  production in the context of the POWHEG BOX [20], a framework for matching dedicated NLO-QCD calculations with public parton-shower programs [21, 22]. We consider both the fully-leptonic and the semi-leptonic decay modes of the  $W$  bosons.

We describe the technical details of our implementation in Sec. 2. Section 3 contains sample phenomenological results for a few representative setups, where the  $W$  bosons decay either fully leptonically or semi-leptonically. In the last case, we consider also a kinematical regime where the  $W$  bosons are produced highly boosted. The code has been made available in the public repository of the POWHEG BOX at the web site <http://powhegbox.mib.infn.it>. Our conclusions are given in Sec. 4.

## 2. Technical details

### 2.1 Next-to-leading order QCD corrections to VBF $W^+W^-jj$ production

The calculation of the next-to-leading order (NLO) QCD corrections to VBF  $W^+W^-jj$  production with fully leptonic decays has first been accomplished in Ref. [11] and is publicly available in the framework of the VBFNLO package [23]. We extracted the matrix elements at Born level, the real emission and the virtual corrections from that reference and adapted them to the format required by the POWHEG BOX. In addition, we are providing matrix elements for the semi-leptonic decays of the weak bosons.

Electroweak  $W^+W^-jj$  production with fully leptonic decays in hadronic collisions mainly proceeds via the scattering of two (anti-)quarks by the exchange of weak bosons in the  $t$ -channel, which in turn emit  $W$  bosons that may decay into lepton-neutrino pairs, c.f. Fig. 1 (a). Furthermore, diagrams with one or both of the weak bosons being emitted off a quark line occur, c. f. Fig. 1 (b), as well as  $t$ -channel configurations with non-resonant  $\ell^+\nu_\ell\ell'^-\bar{\nu}_{\ell'}$  production in addition to the two jets, c. f. Fig. 1 (c). In principle, the same final state may arise from quark-antiquark annihilation diagrams with weak-boson exchange in the  $s$ -channel and subsequent decay of one of the gauge bosons into a pair of jets. Such contributions have been shown to be negligible [15, 24] in regions of phase space

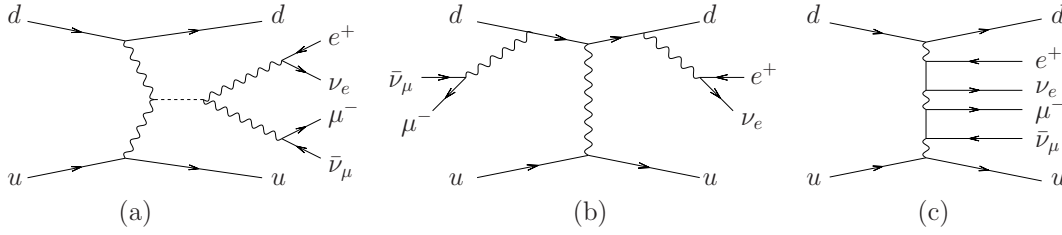


**Figure 1:** Resonant (a,b) and non-resonant (c) sample diagrams for the partonic subprocess  $du \rightarrow e^+ \nu_e \mu^- \bar{\nu}_\mu du$  at leading order.

where VBF processes are searched for experimentally, and will therefore be disregarded throughout. For subprocesses with identical quark-flavor combinations, in addition to the  $t$ -channel topologies one encounters  $u$ -channel exchange diagrams, which we include in our calculation. Their interference with the  $t$ -channel diagrams is however strongly suppressed once typical VBF selection cuts are applied, and will therefore be neglected here.

In the following, we will refer to the electroweak production process  $pp \rightarrow e^+ \nu_e \mu^- \bar{\nu}_\mu jj$  within the above-mentioned approximations as “fully leptonic VBF  $W^+ W^- jj$ ” production, even though we include contributions from non-resonant diagrams that do not arise from the decay of a  $W^+ W^- jj$  intermediate state. Final states related to one of the weak bosons in  $pp \rightarrow W^+ W^- jj$  decaying into a massless quark-antiquark and the other one into a lepton-neutrino pair are referred to as “semi-leptonic”. In analogy to the fully leptonic decay mode, for semi-leptonic VBF  $W^+ W^- jj$  production we take double-, single- and non-resonant diagrams into account and neglect  $s$ -channel contributions as well as interference effects between identical quarks of the VBF production process. In addition, we disregard interference effects between the decay quarks and the quarks of the VBF production process. Decays into massive quarks are not taken into account. For a recent reference on the impact of quark masses in semi-leptonic  $H \rightarrow WW^*$  decays, see, e.g., Ref. [25]. Representative diagrams for the partonic subprocess  $du \rightarrow e^+ \nu_e \mu^- \bar{\nu}_\mu jj$  can be obtained by replacing the  $e^+ \nu_e$  in Fig. 1 with  $c\bar{s}$  pairs. Similarly, some diagrams for the partonic subprocess  $du \rightarrow s\bar{c} \mu^- \bar{\nu}_\mu jj$  are obtained by replacing the  $\mu^- \bar{\nu}_\mu$  in Fig. 1 with  $s\bar{c}$  pairs. We note, however, that some additional diagrams that, because of the absence of a photon-neutrino coupling, do not occur for the  $e^+ \nu_e \mu^- \bar{\nu}_\mu jj$  final state have to be computed for each of the semi-leptonic decay modes.

The NLO-QCD corrections to fully leptonic VBF  $W^+ W^- jj$  production comprise real-emission contributions with one extra parton in the final state and the interference of one-loop diagrams with the Born amplitude. Within our approximations, for the latter only self-energy, triangle, box, and pentagon corrections to either the upper or the lower fermion line have to be considered. The finite parts of these contributions are evaluated numerically by means of a Passarino-Veltman-type tensor reduction that is stabilized by means of the methods of Refs. [26,27]. The numerical stability is monitored by checking Ward identities at every phase-space point. The real-emission contributions are obtained by attaching a gluon in all possible ways to the tree-level diagrams discussed above. Crossing-related diagrams with a gluon in the initial state are also taken into account. Infrared singularities

emerging in both, real-emission and virtual contributions, at intermediate steps of the calculation, are taken care of via the Frixione-Kunszt-Signer subtraction approach [28] that is provided by the **POWHEG BOX** framework. For semi-leptonic VBF  $W^+W^-jj$  production, QCD corrections to the  $W$  hadronic decay are implemented only in the shower approximation. We remark, however, that most shower Monte Carlo programs describe the dressing of hadronic  $W$  decays with QCD radiation accurately, since they have been fit to LEP2 data. The NLO-QCD corrections are thus of the same form as those for the fully leptonic final state, but hadronic decays include the inclusive  $\mathcal{O}(\alpha_s)$  QCD correction to the decay vertex.

## 2.2 The **POWHEG BOX** implementation

For the implementation of VBF  $W^+W^-jj$  production in the framework of the **POWHEG BOX** we proceed in analogy to Refs. [16, 29]. Because of the larger complexity of the current process, however, some further developments are necessary.

As an input, the **POWHEG BOX** requires a list of all independent flavor structures of the Born and the real emission processes, the Born amplitude squared, the real-emission amplitude squared, the finite parts of the virtual amplitudes interfered with the Born, the spin- and the color-correlated Born amplitudes squared. Because of the simple color structure of VBF processes the latter are just multiples of the Born amplitude itself, while the spin-correlated amplitudes vanish entirely. For the fully leptonic decay modes, the LO amplitudes squared, the virtual and the real-emission contributions are extracted from Ref. [11], as described in the previous section. For semi-leptonic decays of the weak bosons, appropriate modifications of the matrix elements are performed. Subtraction terms do not need to be provided explicitly, but are computed by the **POWHEG BOX** internally. Due to the special color structure of VBF processes, within our approximations there is no interference between radiation off the upper and the lower fermion lines. This information has to be passed to the **POWHEG BOX** by assigning a tag to each quark line, as explained in some detail in Refs. [16, 30]. The tags are taken into account by the **POWHEG BOX** when singular regions for the generation of radiation are identified.

Similarly to the case of electroweak  $Zjj$  production [29], in the Born cross section for electroweak  $W^+W^-jj$  production collinear  $q \rightarrow q\gamma$  configurations can arise when a  $t$ -channel photon of low virtuality is exchanged. Such contributions are considered to be part of the QCD corrections to  $p\gamma \rightarrow W^+W^-jj$  and not taken into account here. To effectively remove such contributions even before VBF cuts are applied, we introduce a cut-off variable  $Q_{\gamma,\min}^2 = 4 \text{ GeV}^2$  for the virtuality of the  $t$ -channel exchange boson. Contributions from configurations with a virtuality  $Q^2$  below this cutoff value are dropped prior to phase-space integration. We checked that, within the numerical accuracy of the program, predictions do not change when the cut-off variable is increased to  $10 \text{ GeV}^2$ .

To improve the efficiency of the program, in addition we are employing a so-called Born-suppression factor  $F(\Phi_n)$  that vanishes whenever a singular region of the Born phase space  $\Phi_n$  is approached. In the **POWHEG BOX**, the underlying Born kinematics is then generated

according to a modified  $\bar{B}$  function,

$$\bar{B}_{\text{supp}} = \bar{B}(\Phi_n)F(\Phi_n). \quad (2.1)$$

For VBF  $W^+W^-jj$  production, at Born level, singular configurations related to the exchange of a photon of low virtuality in the  $t$ -channel are characterized by low transverse momentum of an outgoing parton. It is therefore advantageous to apply a Born-suppression factor that damps such configurations. Following the prescription of Ref. [29], we are using

$$F(\Phi_n) = \left( \frac{p_{T,1}^2}{p_{T,1}^2 + \Lambda^2} \right)^2 \left( \frac{p_{T,2}^2}{p_{T,2}^2 + \Lambda^2} \right)^2, \quad (2.2)$$

with the  $p_{T,i}$  denoting the transverse momenta of the two outgoing partons of the underlying Born configuration, and  $\Lambda = 10$  GeV.

Electroweak  $W^+W^-$  production in association with two jets contains contributions from VBF-induced Higgs production with subsequent decay into a pair of weak bosons, and from continuum  $W^+W^-$  production via VBF. These two types of contributions populate different regions of phase space: The Higgs resonance exhibits a pronounced peak where the invariant mass of the decay leptons and neutrinos,  $M_{\text{decay}}$ , is equal to the Higgs mass, whereas the  $WW$  continuum is distributed over a broad range in  $M_{\text{decay}}$ . In order to optimize the efficiency of the phase space integration, in the case of a light Higgs boson with a narrow width we have split our simulation into two contributions, depending on the value of  $M_{\text{decay}}$  in the underlying Born configuration. In the region

$$m_H - n \cdot \Gamma_H < M_{\text{decay}} < m_H + n \cdot \Gamma_H, \quad n = 50, \quad (2.3)$$

our results are then dominated by the sharp Higgs resonance, whereas for other values of  $M_{\text{decay}}$  results are fully dominated by the broad  $WW$  continuum. Even though both phase space regions contain contributions from all Feynman diagrams, for simplicity we refer to the region of Eq. (2.3) as “Higgs resonance” and to the complementary region as “ $WW$  continuum”.

We note that, because of the presence of two neutrinos, the invariant mass distribution cannot be fully reconstructed in experiment in the fully leptonic decay mode. The separation we perform is of purely technical nature and serves the only purpose of improving the convergence of the phase space integration. To obtain meaningful results for the full VBF  $W^+W^-jj$  final state, the two contributions therefore have to be added, and results are independent of the choice of  $n$  in Eq. (2.3). Still, it is interesting to observe the differences of some characteristic distributions in these two regions. Figure 2 shows the azimuthal angle separation of the two charged leptons after only basic transverse momentum cuts of  $p_{T,j} > 25$  GeV are applied on the two hardest jets that are reconstructed via the anti- $k_T$  algorithm [31, 32] in the rapidity range  $y_j < 4.5$ , with  $R > 0.4$ . As is evident, in the Higgs resonance region the leptons tend to be close in azimuthal angle, as they arise from the decay of two weak bosons that stem from a Higgs boson of spin zero. In the continuum region, no such correlation exists between the decay leptons, resulting in a completely different shape of the angular distribution [33]. Should one wish to enhance

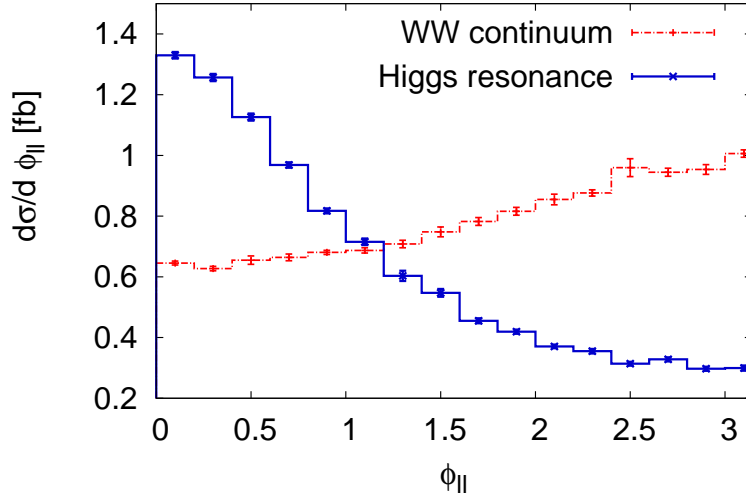


**Figure 2:** Azimuthal angle separation of the two charged leptons at NLO-QCD accuracy for the Higgs resonance and the  $W^+W^-$  continuum region. See text for more details.

the Higgs contributions with respect to the full VBF  $W^+W^-jj$  cross section, clearly one would make use of this feature.

In order to validate the complete implementation of VBF  $W^+W^-jj$  production in the `POWHEG BOX`, we have performed various checks. The LO and real-emission matrix elements for each class of subprocesses have been compared at the amplitude level to `MadGraph`-generated code [34, 35]. We found agreement at the level of 12 significant digits. With the user-supplied LO and real-emission matrix elements squared, the `POWHEG BOX` itself tests whether the real-emission cross section approaches all soft and collinear limits correctly. This provides a useful check on the relative normalization of the Born and real-emission amplitudes squared as well as on the flavor summation. For the fully leptonic decay mode, we have furthermore compared all parts of the NLO-QCD calculation to the respective results generated with the code of Ref. [11]. We found full agreement for integrated cross sections and differential distributions at LO and at NLO-QCD, both within inclusive cuts and after imposing VBF-specific selection criteria.

Finally, we remark that in order to produce the plots presented in this work, we have used a new version of the `POWHEG BOX` files that were kindly provided to us by Paolo Nason and that will soon be released as part of the Version 2 of the `POWHEG BOX`. In particular these files allow to compute the integration grids in parallel and have a more efficient calculation of the upper bounds.

### 3. Phenomenological results

Our implementation of VBF  $W^+W^-jj$  production in the `POWHEG BOX` is publicly available. Instructions for downloading the code are available from the the web site of the `POWHEG BOX` project, <http://powhegbox.mib.infn.it>. Technical parameters of the code and recommendations for its use can be found in a documentation that is provided together with the code. In this article, we present results obtained with our `POWHEG BOX` implementation

for some representative setups. The user of the POWHEG BOX is of course free to perform studies with settings of her own choice.

### 3.1 Results at 8 TeV

We consider proton-proton collisions at a center-of mass energy of  $\sqrt{s} = 8$  TeV. For the parton distribution functions of the proton we use the NLO set of the MSTW2008 parametrization [36], as implemented in the LHAPDF library [37]. Jets are defined according to the anti- $k_T$  algorithm [31,32] with  $R = 0.4$ , making use of the FASTJET package [38]. As electroweak (EW) input parameters we use the mass of the  $Z$  boson,  $m_Z = 91.188$  GeV, the mass of the  $W$  boson,  $m_W = 80.419$  GeV, and the Fermi constant,  $G_F = 1.16639 \times 10^{-5}$  GeV $^{-1}$ . Other EW parameters are obtained from these via tree-level electroweak relations. For the widths of the weak bosons we use  $\Gamma_Z = 2.51$  GeV,  $\Gamma_W = 2.099$  GeV. In case semi-leptonic decay modes are considered, the hadronic width is corrected with a factor  $[1 + \alpha_s(m_W)/\pi]$ . The factorization and renormalization scales are set to  $\mu_F = \mu_R = m_W$  throughout.

#### 3.1.1 Fully leptonic decay mode

VBF  $W^+W^-jj$  production with fully leptonic decays of the  $W$  bosons is an important channel in the Higgs search over a wide mass range. Here, we present numerical results for electroweak  $e^+\nu_e\mu^-\bar{\nu}_\mu jj$  production at the LHC within the setup outlined above. The mass of the Higgs boson is set to  $m_H = 125$  GeV, the region where the ATLAS and CMS collaborations observe a new resonance compatible with the Higgs boson predicted by the Standard Model [1, 2]. The width of the Higgs boson is set to  $\Gamma_H = 0.00498$  GeV. Our phenomenological study is inspired by the analysis strategy of Ref. [39]. We require the presence of two jets with

$$p_{T,j} > 25 \text{ GeV}, \quad y_j < 4.5. \quad (3.1)$$

The two hardest jets inside the considered rapidity range are referred to as “tagging jets”. These two tagging jets are furthermore required to be well-separated from each other,

$$|y_{j1} - y_{j2}| < 3.8, \quad y_{j1} \times y_{j2} < 0, \quad m_{j1j2} > 500 \text{ GeV}. \quad (3.2)$$

We require missing energy and two hard charged leptons in the central rapidity region,

$$y_\ell < 2.5, \quad p_{T,\ell_1} > 25 \text{ GeV}, \quad p_{T,\ell_2} > 15 \text{ GeV}, \quad p_T^{\text{miss}} > 25 \text{ GeV}, \quad (3.3)$$

which are well-separated from each other and from the jets,

$$R_{\ell\ell} > 0.3, \quad R_{j\ell} > 0.3, \quad (3.4)$$

but close in azimuthal angle,

$$|\phi_{\ell_1} - \phi_{\ell_2}| < 1.8, \quad (3.5)$$

and located in the rapidity region between the two tagging jets,

$$\min\{y_{j1}, y_{j2}\} < y_\ell < \max\{y_{j1}, y_{j2}\}. \quad (3.6)$$



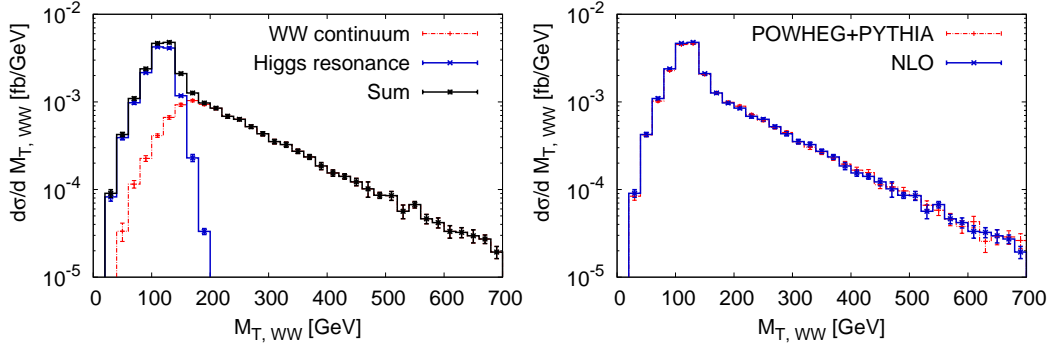


**Figure 3:** Transverse mass distribution of the four-lepton system, as defined in Eq. (3.7), for  $pp \rightarrow e^+ \nu_e \mu^- \bar{\nu}_\mu jj$  at the LHC with  $\sqrt{s} = 8$  TeV within the VBF cuts of Eqs. (3.1)–(3.6). Left panel: results at NLO-QCD accuracy for the Higgs resonance (blue line), the  $WW$  continuum (red line), and their sum (black line). Right panel: Sum of the two contributions at NLO-QCD (blue solid lines) and with POWHEG+PYTHIA (red dashed lines).

When these cuts are applied, the inclusive cross section contributions for VBF  $e^+ \nu_e \mu^- \bar{\nu}_\mu jj$  production given in Sec. 2 are given by  $\sigma_{WW}^{\text{VBF}} = (0.202 \pm 0.002)$  fb and  $\sigma_{\text{Higgs}}^{\text{VBF}} = (0.268 \pm 0.003)$  fb at NLO-QCD, amounting to a total of  $\sigma^{\text{VBF}} = (0.470 \pm 0.003)$  fb. Because of our selection cuts, in particular the cut on the azimuthal angle separation of the charged leptons, Eq. (3.5), the Higgs contribution is slightly preferred compared to the  $WW$  continuum. The VBF cross section at NLO QCD changes by less than 2% when the factorization and renormalization scales are varied simultaneously in the range  $\mu_F = \mu_R = m_W/2$  to  $2m_W$ . Slightly larger scale uncertainties are found for distributions related to jets that are emitted in addition to the two tagging jets. As such jets can first occur via the real-emission contributions of the NLO calculation, their kinematic properties are effectively described at LO only, and thus plagued by larger scale uncertainties than true NLO observables. While our calculation has been performed for a fixed choice of scale that should facilitate comparison to future calculations, we mention that more sophisticated choices are possible with our code, for instance like those suggested in the context of the MINLO method [40].

Since the invariant mass of the  $e^+ \nu_e \mu^- \bar{\nu}_\mu$  system cannot be fully reconstructed, it is common to consider the transverse mass instead, which is defined as

$$m_{T,WW} = \sqrt{(E_T^{\ell\ell} + E_T^{\text{miss}})^2 - |\vec{p}_T^{\ell\ell} + \vec{p}_T^{\text{miss}}|^2}, \quad \text{with } E_T^{\ell\ell} = \sqrt{|\vec{p}_T^{\ell\ell}|^2 + m_{\ell\ell}^2}. \quad (3.7)$$

Figure 3 (a) shows the respective contributions to  $d\sigma^{\text{VBF}}/dm_{T,WW}$  of the Higgs resonance and of the  $WW$  continuum, as defined in Sec. 2, as well as their sum. The Higgs contribution is peaked at  $m_{T,WW} \sim m_H$ , while the  $WW$  continuum is largest in the kinematic range where two weak bosons can be produced on-shell.

In Fig. 3 (b), we show the transverse mass distribution at pure NLO QCD, as well as at NLO matched with a parton-shower program via POWHEG (NLO+PS). For the parton shower, here and in the following we are using PYTHIA 6.4.25 [19] with the Perugia 0 tune for the shower, including hadronization corrections, multi-parton interactions and underlying event. We do not take QED radiation effects into account. The shape of the transverse mass

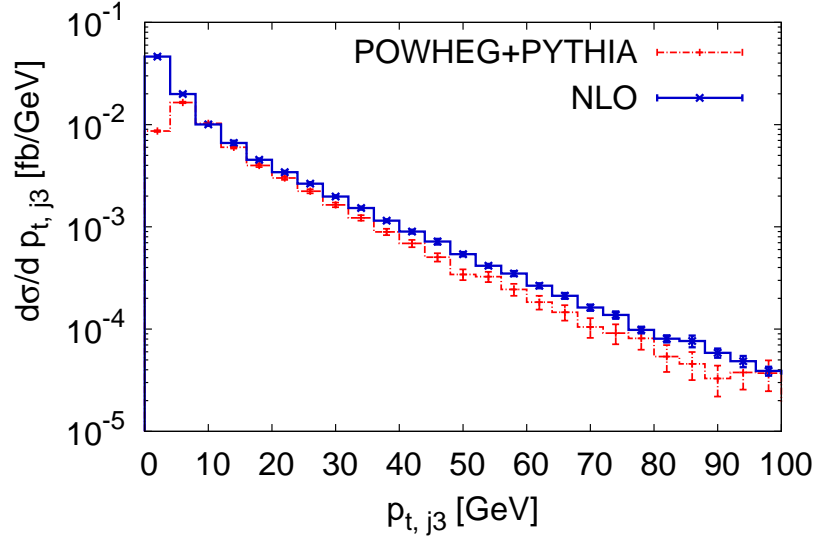


**Figure 4:** Transverse momentum distribution of the third jet in  $pp \rightarrow e^+ \nu_e \mu^- \bar{\nu}_\mu jj$  at the LHC within the VBF cuts of Eqs. (3.1)–(3.6) at NLO-QCD (blue solid lines) and with POWHEG+PYTHIA (red dashed lines).

distribution is only barely affected by parton-shower effects. Similarly small distortions of shapes are observed for the transverse momentum and rapidity distributions of the leptons, as well as for their azimuthal angle separation. The overall normalization of the VBF cross sections decreases by about 2% when the NLO calculation is combined with PYTHIA. The parton shower mostly gives rise to the emission of soft or collinear radiation, while the probability for the emission of *hard* extra jets does not increase because of parton-shower effects. Indeed, the production rate of a third hard jet decreases when the NLO calculation is merged with PYTHIA, as illustrated in Fig. 4, which shows the transverse momentum distribution of the third jet in  $pp \rightarrow e^+ \nu_e \mu^- \bar{\nu}_\mu jj$  at NLO QCD and for POWHEG+PYTHIA. At NLO, only the real-emission contributions can give rise to a third jet. Distributions related to this jet are thus effectively described only at the lowest non-vanishing order in the fixed-order predictions, while in the POWHEG+PYTHIA results soft-collinear radiation is resummed at leading-logarithmic accuracy via the Sudakov factor, resulting in a damping of contributions with very small  $p_{T,j3}$ .

A quantitative understanding of central jets that are located in between the two tagging jets is of crucial importance for the discrimination of VBF events from hard QCD processes as well as from underlying event and pile-up effects at the LHC. These backgrounds are characterized by a considerable amount of jet activity in the central-rapidity region of the detector, whereas the emission of hard jets at central rapidities is strongly suppressed in VBF processes. Figure 5 shows the rapidity distribution of the third jet in VBF-induced  $e^+ \nu_e \mu^- \bar{\nu}_\mu jj$  production at the LHC. Obviously, the shape of the NLO-QCD distributions is not particularly sensitive to the transverse momentum cut imposed on the third jet. However, when the NLO calculation is merged with PYTHIA, the central-rapidity region is considerably filled by extra jets, as illustrated in the left panel of Fig. 5, where in addition

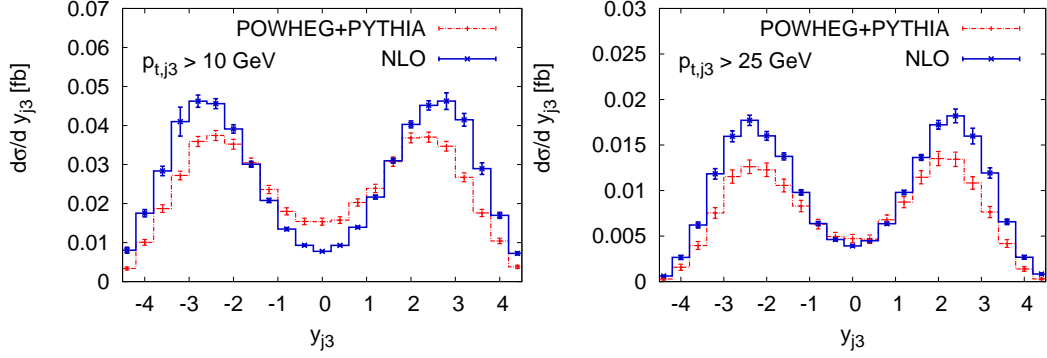


**Figure 5:** Rapidity distribution of the third jet in  $pp \rightarrow e^+ \nu_e \mu^- \bar{\nu}_\mu jj$  at the LHC within the VBF cuts of Eqs. (3.1)–(3.6) and an additional cut of  $p_{T,j_3} > 10$  GeV (left panel) and  $p_{T,j_3} > 25$  GeV (right panel), respectively, at NLO-QCD (blue solid lines) and with POWHEG+PYTHIA (red dashed lines).

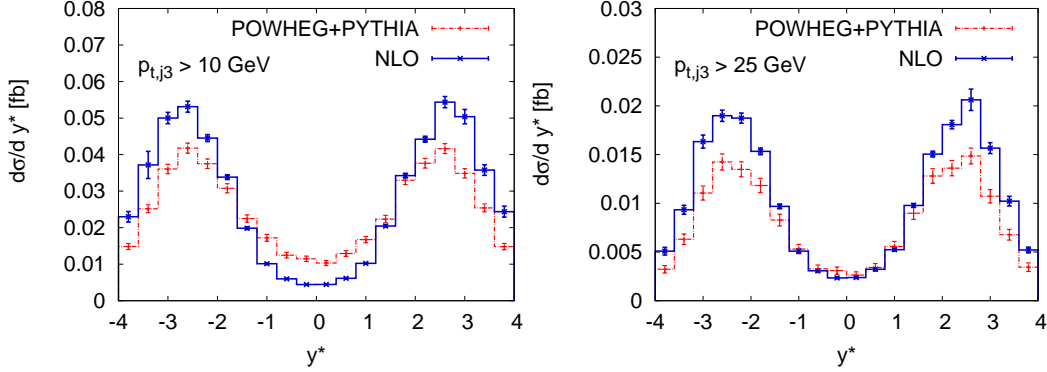


**Figure 6:** Rapidity distribution of the third jet with respect to the average of the two tagging jets in  $pp \rightarrow e^+ \nu_e \mu^- \bar{\nu}_\mu jj$  at the LHC within the VBF cuts of Eqs. (3.1)–(3.6), and an additional cut of  $p_{T,j_3} > 10$  GeV (left panel) and  $p_{T,j_3} > 25$  GeV (right panel), respectively, at NLO-QCD (blue solid lines) and with POWHEG+PYTHIA (red dashed lines).

to the VBF cuts of Eqs. (3.1)–(3.6) we impose a loose cut of  $p_{T,j_3} > 10$  GeV on the third-hardest jet. A significant reduction of the central-jet activity can be achieved by tightening this cut to  $p_{T,j_3} > 25$  GeV, as shown in the right panel of the same figure.

The relative position of the third jet with respect to the two tagging jets is accessible via the variable

$$y^* = y_{j_3} - \frac{y_{j_1} + y_{j_2}}{2}. \quad (3.8)$$

In Fig. 6 (a) the  $y^*$  distribution is shown within the VBF cuts of Eqs. (3.1)–(3.6) and with two different cuts on the third jet,  $p_{T,j_3} > 10$  GeV and  $p_{T,j_3} > 25$  GeV, respectively. As for the rapidity distribution of the third jet, we observe that the parton shower tends to fill the central region. Increasing the transverse momentum cut of the third jet reduces this central activity.

Central-jet veto techniques [7, 8, 41] are based on the observation that QCD backgrounds can be suppressed efficiently, if one rejects events with one or more hard jets

between the two tagging jets, for instance, with

$$p_T^{j,\text{veto}} < 20 \text{ GeV}, \quad \min\{y_{j1}, y_{j2}\} < y_{j,\text{veto}} < \max\{y_{j1}, y_{j2}\}. \quad (3.9)$$

Because of the small amount of jet activity in the central region, this central-jet veto diminishes the VBF signal only marginally, resulting in a decrease of about 12% in the NLO and NLO+PS cross sections.

### 3.1.2 Semi-leptonic decay mode

While fully leptonic decays of a Higgs boson produced via VBF give rise to a rather clean final state with little jet activity in the central-rapidity region, the invariant mass of the system consisting of two charged leptons and two neutrinos cannot be fully reconstructed. For Higgs masses above the  $W$ -pair production threshold, the  $H \rightarrow WW \rightarrow \ell\nu jj$  channel, with one of the weak bosons decaying into a pair of jets, while the other one decays into a lepton-neutrino pair, thus becomes interesting. In this channel, the invariant mass of the decay system can be reconstructed, using kinematical constraints to estimate the longitudinal component of the neutrino momentum. A recent search for a Higgs boson in the range  $300 \leq m_H \leq 600 \text{ GeV}$  by the ATLAS collaboration [42] is thus based on the  $\ell\nu jj$  final state.

Here, we wish to show some representative results for VBF  $W^+W^-jj$  production with semi-leptonic decays of the weak bosons in the presence of one heavy Higgs boson, following closely the analysis strategy of Ref. [42]. For the Higgs boson we assume a mass of  $m_H = 400 \text{ GeV}$  and a width of  $\Gamma_H = 26.791 \text{ GeV}$ .

We require the presence of at least four hard jets with transverse momenta larger than 25 GeV. The decay jets of the hadronically decaying  $W$  boson are then identified as the pair of two out of the four hardest jets whose invariant mass is closest to  $m_W$ . If we do not find a pair of jets in the range

$$71 \text{ GeV} \leq m_{jj}^{\text{dec}} \leq 91 \text{ GeV}, \quad (3.10)$$

we discard the respective event. The remaining two hardest jets with

$$p_{T,j} > 25 \text{ GeV}, \quad y_j < 4.5, \quad (3.11)$$

are identified as the tagging jets, which have to fulfill the following requirements:

$$|y_{j1} - y_{j2}| < 3, \quad y_{j1} \times y_{j2} < 0, \quad m_{j1j2} > 600 \text{ GeV}. \quad (3.12)$$

In addition, we require a hard lepton and large missing energy,

$$p_{T,\ell} > 30 \text{ GeV}, \quad p_T^{\text{miss}} > 30 \text{ GeV}. \quad (3.13)$$

The tagging jets have to be well-separated from the hard charged lepton and from the decay jets,

$$R_{j\ell} > 0.3, \quad R_{jd} > 0.3, \quad (3.14)$$

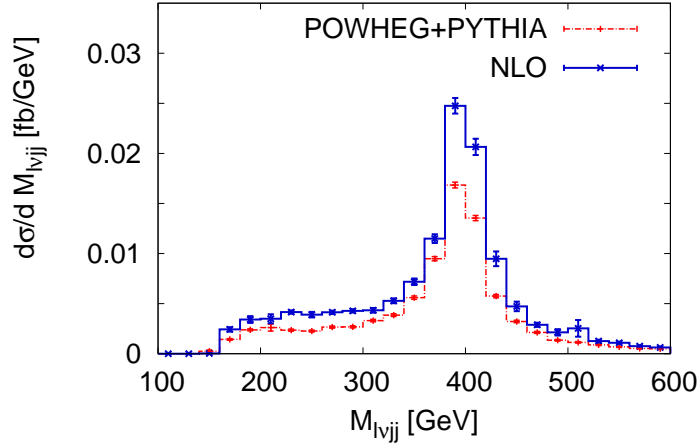


**Figure 7:** Invariant-mass distribution of the decay system in  $pp \rightarrow W^+(jj)W^-(\mu^-\bar{\nu}_\mu)jj$  at the LHC within the VBF cuts of Eqs. (3.10)–(3.15), at NLO-QCD (blue solid lines) and with POWHEG+PYTHIA (red dashed lines), see text for details.

Both, the decay jets and the hard charged lepton have to be located in the rapidity range between the two tagging jets,

$$\min\{y_{j1}, y_{j2}\} < y_\ell, y_j^{\text{dec}} < \max\{y_{j1}, y_{j2}\}. \quad (3.15)$$

In contrast to the fully leptonic decay modes, the invariant mass of the decay system can be reconstructed, if the  $W$  bosons are produced on-shell. Following the prescription of Ref. [42], for each event the transverse component of the neutrino is identified with the missing transverse energy. The longitudinal momentum of the neutrino is computed via the quadratic equation given by the mass constraint  $m_{\ell\nu} = m_W$ . In case of two real solutions, the solution resulting in a smaller longitudinal neutrino momentum component,  $|p_\nu^z|$ , is taken. In case of complex solutions, the event is disregarded. Figure 7 shows the invariant mass of the decay system,  $M_{\ell\nu jj}$ , with the neutrino momentum reconstructed as described above. The peak of  $M_{\ell\nu jj}$  at the value of the heavy Higgs boson’s mass,  $m_H = 400$  GeV, is clearly visible at NLO QCD. Its position is retained in the POWHEG+PYTHIA result. However the normalization of the distribution is modified considerably when the NLO calculation is merged with PYTHIA. This effect can be traced back to a reduction of the cross section for semi-leptonic VBF  $W^+W^-jj$  production within the above cuts, by about 30% when going from NLO to NLO+PS. This large difference can be explained by observing that invariant mass distributions receive very large corrections from the parton shower. Indeed, in the setup of ref. [42], that we adopted here, one requires the invariant mass of the two jets stemming from the  $W$  decay to be still close to the  $W$  mass after parton showering. However, the soft radiation from the parton shower tends to smear this mass distribution, and, as a consequence, a large number of events are discarded since they do not satisfy the condition in Eq. (3.10). A way to avoid these large corrections is to consider a kinematical regime where the  $W$  bosons are highly boosted and decay into a single fat jet. In this case, jet-substructure techniques can be used to distinguish the jets coming from the  $W$  decay from the other jets. We outline such a study in the next section.

### 3.2 Semi-leptonic decay mode with boosted kinematics

At the LHC, in particular when it is running at its design energy of  $\sqrt{s} = 14$  TeV (or close to it), heavy particles are copiously produced with transverse momenta that greatly exceed their rest mass. These boosted objects give rise to highly collimated streams of decay particles in the detector. It is then useful to exploit the feature that the partons formed in the decay of the boosted object are close to each other, and, with a suitable jet-algorithm, will end up in one single jet. Modern jet deconstruction techniques have been designed to resolve the substructure of the so-called *fat jet* that arises from the hadronic decay of the heavy, boosted object and to discriminate this jet from ordinary QCD jets (see, e.g., Ref. [43] for a recent review).

We here present an analysis of electroweak  $W^+W^-jj$  production, assuming the presence of just a light Higgs boson with  $m_H = 125$  GeV, in the kinematic regime that is particularly interesting in the context of weak boson scattering. Possible new physics in the gauge boson sector is expected to manifest itself in the scattering of the longitudinal gauge boson modes,  $W_L W_L \rightarrow W_L W_L$ , at high energies. To access this region in VBF  $W^+W^-jj$  production with semi-leptonic decays of the weak bosons, we closely follow the strategy of Ref. [44], supplemented by the jet-filtering techniques of Ref. [45]. We require the presence of a highly-boosted jet with

$$p_{T,j}^{\text{boosted}} > 300 \text{ GeV}, \quad (3.16)$$

which is constructed with  $R = 1.0$  using the Cambridge/Aachen algorithm [46, 47] for flexibly resolving different angular scales. Similar to what is done in Ref. [45] we look for a boosted jet with invariant mass  $M_J$  close to the mass of the  $W$  boson,

$$m_W - 10 \text{ GeV} < M_J < m_W + 10 \text{ GeV}. \quad (3.17)$$

To ensure that this fat jet is related to the decay of a heavy boosted gauge boson, we additionally investigate its composition and demand that it consists of two subjets  $J_1, J_2$  with invariant masses  $m_{J_1} < m_{J_2}$ . If there is a significant mass drop with respect to the fat jet,

$$m_{J_1} < 0.67 \cdot M_J, \quad \text{and} \quad y = \frac{\min(p_{T,J_1}^2, p_{T,J_2}^2)}{M_J^2} \Delta R_{J_1, J_2} > 0.09, \quad (3.18)$$

the boosted jet is deemed compatible with the  $W$ -decay. If no jet in the event satisfies these cuts, the event is discarded. The remaining two hardest jets with

$$p_{T,j} > 25 \text{ GeV}, \quad y_j < 4.5, \quad (3.19)$$

are identified as the tagging jets, which have to fulfill the following requirements:

$$|y_{j1} - y_{j2}| < 3, \quad y_{j1} \times y_{j2} < 0, \quad m_{j1j2} > 600 \text{ GeV}. \quad (3.20)$$

The hardest lepton also is forced into the boosted regime by the transverse momentum cut

$$p_{T,\ell} > 300 \text{ GeV}. \quad (3.21)$$

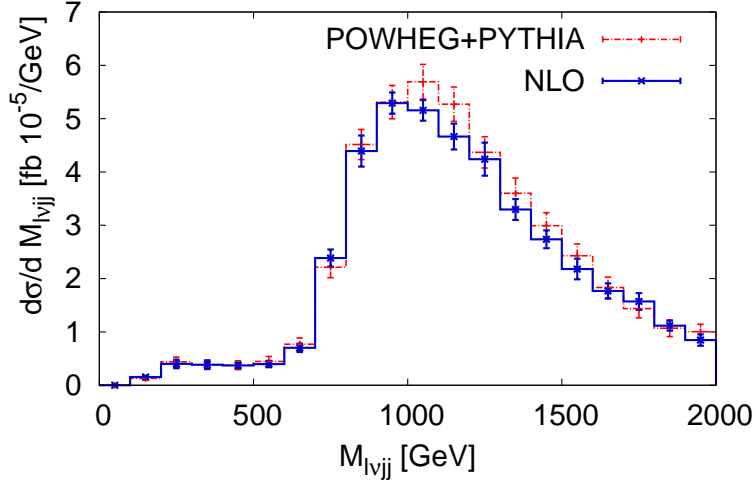


**Figure 8:** Invariant-mass distribution of the decay system in  $pp \rightarrow W^+(jj)W^-(\mu^-\bar{\nu}_\mu)jj$  at the LHC with  $\sqrt{s} = 14$  TeV for the boosted kinematics within the cuts of Eqs. (3.16)–(3.23), at NLO-QCD (blue solid lines) and with POWHEG+PYTHIA (red dashed lines), see text for details.

The longitudinal momentum component of the neutrino is computed in the same way as in the analysis described in Sec. 3.1.2. In addition, we require

$$p_T^{\text{miss}} > 30 \text{ GeV}, \quad R_{j\ell} > 0.3. \quad (3.22)$$

with the latter denoting the  $R$ -separation between the tagging jets  $j$  and the lepton. The lepton and the fat jet need to be located in between the two tagging jets,

$$\min\{y_{j1}, y_{j2}\} < y_\ell, y_{\text{fat}} < \max\{y_{j1}, y_{j2}\}. \quad (3.23)$$

Within this setup, rather small cross sections are obtained, amounting to  $\sigma^{\text{NLO}} = (0.0458 \pm 0.0006)$  fb at NLO. Nonetheless, Ref. [44] suggests that with  $100 \text{ fb}^{-1}$  of luminosity at 14 TeV the LHC can distinguish between  $WW$  scattering in the Standard Model and in scenarios of new physics with extra heavy scalar or vector resonances. The invariant mass distribution of the  $WW$  system is particularly interesting in this context. We show this distribution in Fig. 8 at NLO and at POWHEG+PYTHIA level. Because of the tight cuts imposed, this distribution peaks in the 1 TeV-region. As expected, the impact of the parton shower on the NLO results is comfortably moderate, as apparent from the small differences between the respective curves in the figure. The transverse momentum and rapidity distributions of the tagging jets and the hard lepton are similarly insensitive to parton-shower effects.

## 4. Conclusions

In this work we have presented an implementation of electroweak  $W^+W^-jj$  production at hadron colliders in the POWHEG-BOX, a framework that allows the merging of NLO-QCD calculations with transverse-momentum ordered parton shower programs such as PYTHIA.

We are providing code for fully leptonic and semi-leptonic decay modes of the weak bosons, taking resonant and non-resonant contributions and spin-correlations of the final-state particles into account. Our implementation is publicly available from the POWHEG-BOX webpage, <http://powhegbox.mib.infn.it>.

While the user of the code is free to set parameters and analysis cuts according to her own needs, we have presented phenomenological results for three representative setups, which are of particular relevance for understanding the mechanism of electroweak symmetry breaking realized in nature. We have investigated VBF  $W^+W^-jj$  production with fully leptonic decays of the weak bosons in the presence of a light Higgs boson, and in a scenario with a heavy Higgs boson and semi-leptonic decays of the weak bosons. In addition, we considered electroweak  $W^+W^-jj$  production in the kinematic regime where the weak bosons are highly boosted and the hadronically decaying  $W$  boson, ending up in a fat jet, is identified via modern jet deconstruction techniques.

We found that the impact of the parton shower on most NLO distributions is moderate in the fully leptonic decay mode, but some care is needed in the definition of observables that are important for central-jet veto techniques. When considering semi-leptonic decay modes, however, significant differences arise between results at NLO QCD and NLO results matched with PYTHIA, unless boosted techniques are used. These systematic differences should be kept in mind when employing VBF  $W^+W^-jj$  production for precision studies at the LHC.

**Acknowledgments** We are grateful to Andrea Banfi, Paolo Nason and Gavin Salam for extensive, valuable discussions. The work of B. J. is supported by the Research Center *Elementary Forces and Mathematical Foundations (EMG)* of the Johannes-Gutenberg-Universität Mainz. G. Z. is supported by the British Science and Technology Facilities Council, by the LHCPHenoNet network under the Grant Agreement PITN-GA-2010-264564 and by the European Research and Training Network (RTN) grant Unification in the LHC ERA under the Agreement PITN-GA-2009-237920.

## References

- [1] G. Aad *et al.* [ATLAS Collaboration], Phys. Lett. B **716** (2012) 1 [arXiv:1207.7214 [hep-ex]].
- [2] S. Chatrchyan *et al.* [CMS Collaboration], Phys. Lett. B **716** (2012) 30 [arXiv:1207.7235 [hep-ex]].
- [3] T. Aaltonen *et al.* [CDF and D0 Collaborations], Phys. Rev. Lett. **109** (2012) 071804 [arXiv:1207.6436 [hep-ex]].
- [4] D. Zeppenfeld, R. Kinnunen, A. Nikitenko and E. Richter-Was, Phys. Rev. D **62** (2000) 013009 [hep-ph/0002036].
- [5] M. Dührssen, S. Heinemeyer, H. Logan, D. Rainwater, G. Weiglein and D. Zeppenfeld, Phys. Rev. D **70** (2004) 113009 [hep-ph/0406323].
- [6] LHC Higgs Cross Section Working Group, A. David, A. Denner, M. Dührssen, M. Grazzini, C. Grojean, G. Passarino and M. Schumacher *et al.*, arXiv:1209.0040 [hep-ph].
- [7] D. L. Rainwater and D. Zeppenfeld, Phys. Rev. D **60** (1999) 113004 [Erratum-ibid. D **61** (2000) 099901] [hep-ph/9906218].



- [8] N. Kauer, T. Plehn, D. L. Rainwater and D. Zeppenfeld, Phys. Lett. B **503** (2001) 113 [hep-ph/0012351].
- [9] D. L. Rainwater and D. Zeppenfeld, JHEP **9712** (1997) 005 [hep-ph/9712271].
- [10] D. L. Rainwater, D. Zeppenfeld and K. Hagiwara, Phys. Rev. D **59** (1998) 014037 [hep-ph/9808468].
- [11] B. Jäger, C. Oleari, D. Zeppenfeld, JHEP **07** (2006) 015. [arXiv:hep-ph/0603177].
- [12] B. Jäger, C. Oleari, D. Zeppenfeld, Phys. Rev. **D73** (2006) 113006. [arXiv:hep-ph/0604200].
- [13] G. Bozzi, B. Jäger, C. Oleari, D. Zeppenfeld, Phys. Rev. **D75** (2007) 073004. [arXiv:hep-ph/0701105].
- [14] B. Jäger, C. Oleari, D. Zeppenfeld, Phys. Rev. **D80** (2009) 034022. [arXiv:0907.0580 [hep-ph]].
- [15] A. Denner, L. Hosekova and S. Kallweit, arXiv:1209.2389 [hep-ph].
- [16] B. Jager and G. Zanderighi, JHEP **1111** (2011) 055 [arXiv:1108.0864 [hep-ph]].
- [17] G. Marchesini *et al.*, Comp. Phys. Commun. **67** (1992) 465.
- [18] G. Corcella *et al.*, JHEP **0101** (2001) 010. [hep-ph/0011363].
- [19] T. Sjostrand, S. Mrenna, P. Z. Skands, JHEP **0605** (2006) 026. [hep-ph/0603175].
- [20] S. Alioli, P. Nason, C. Oleari, E. Re, JHEP **1006** (2010) 043. [arXiv:1002.2581 [hep-ph]].
- [21] P. Nason, JHEP **0411** (2004) 040. [hep-ph/0409146].
- [22] S. Frixione, P. Nason, C. Oleari, JHEP **0711** (2007) 070. [arXiv:0709.2092 [hep-ph]].
- [23] K. Arnold *et al.*, Comp. Phys. Comm. **180** (2009) 1661. [arXiv:0811.4559 [hep-ph]];  
K. Arnold *et al.*, arXiv:1107.4038 [hep-ph];  
K. Arnold *et al.*, arXiv:1207.4975 [hep-ph].
- [24] M. Ciccolini, A. Denner, S. Dittmaier, Phys. Rev. **D77** (2008) 013002. [arXiv:0710.4749 [hep-ph]].
- [25] S. Groote, J. G. Korner and P. Tuvike, arXiv:1301.0881 [hep-ph].
- [26] A. Denner, S. Dittmaier, Nucl. Phys. **B658** (2003) 175. [hep-ph/0212259].
- [27] A. Denner, S. Dittmaier, Nucl. Phys. **B734** (2006) 62. [hep-ph/0509141].
- [28] S. Frixione, Z. Kunszt, A. Signer, Nucl. Phys. **B467** (1996) 399. [hep-ph/9512328].
- [29] B. Jager, S. Schneider, G. Zanderighi, JHEP **1209** (2012) 083 [arXiv:1207.2626 [hep-ph]].
- [30] P. Nason, C. Oleari, JHEP **1002** (2010) 037. [arXiv:0911.5299 [hep-ph]].
- [31] M. Cacciari, G. P. Salam, Phys. Lett. **B641** (2006) 57. [hep-ph/0512210].
- [32] M. Cacciari, G. P. Salam and G. Soyez, JHEP **0804** (2008) 063 [arXiv:0802.1189 [hep-ph]].
- [33] M. Dittmar and H. K. Dreiner, Phys. Rev. D **55** (1997) 167 [hep-ph/9608317].
- [34] T. Stelzer and W. F. Long, Comput. Phys. Commun. **81** (1994) 357 [hep-ph/9401258].
- [35] J. Alwall *et al.*, JHEP **0709** (2007) 028 [arXiv:0706.2334 [hep-ph]].

- [36] A. D. Martin, W. J. Stirling, R. S. Thorne, G. Watt, Eur. Phys. J. **C63** (2009) 189-285. [arXiv:0901.0002 [hep-ph]].
- [37] M. R. Whalley, D. Bourilkov, R. C. Group, hep-ph/0508110.
- [38] M. Cacciari, G. P. Salam and G. Soyez, Eur. Phys. J. C **72** (2012) 1896 [arXiv:1111.6097 [hep-ph]].
- [39] ATLAS Collaboration,  
<http://cdsweb.cern.ch/record/1462530/files/ATLAS-CONF-2012-098>,  
 ATLAS-CONF-2012-098 (2012).
- [40] K. Hamilton, P. Nason and G. Zanderighi, JHEP **1210** (2012) 155 [arXiv:1206.3572 [hep-ph]].
- [41] V. D. Barger, R. J. N. Phillips and D. Zeppenfeld, Phys. Lett. B **346** (1995) 106 [hep-ph/9412276].
- [42] G. Aad *et al.* [ATLAS Collaboration], arXiv:1206.6074 [hep-ex].
- [43] A. Abdesselam *et al.*, Eur. Phys. J. C **71** (2011) 1661 [arXiv:1012.5412 [hep-ph]].
- [44] J. M. Butterworth, B. E. Cox and J. R. Forshaw, Phys. Rev. D **65** (2002) 096014 [hep-ph/0201098].
- [45] J. M. Butterworth, A. R. Davison, M. Rubin and G. P. Salam, Phys. Rev. Lett. **100** (2008) 242001 [arXiv:0802.2470 [hep-ph]].
- [46] Y. L. Dokshitzer, G. D. Leder, S. Moretti and B. R. Webber, JHEP **9708** (1997) 001 [hep-ph/9707323].
- [47] M. Wobisch and T. Wengler, In \*Hamburg 1998/1999, Monte Carlo generators for HERA physics\* 270-279 [hep-ph/9907280].